

EFFECTS OF REGULARLY ARRAYED ROUGHNESS ON FLOW RESISTANCE AND TURBULENT FLOW STRUCTURE IN AN OPEN CHANNEL

Sukarno

Department of Civil Engineering Sam Ratulangi University

Jln. Kampus Bahu Unsrat Manado

E-mail: sukarno091@yahoo.com

ABSTRACT

Effects of regularly arrayed cylindrical and sphere roughness on flow resistance and turbulent characteristics in an open channel have been investigated over a completely rough-bed with uniform stainless steel rods and glass beads. Detailed spatial measurements of streamwise and vertical velocity fluctuations were conducted using Particle Image Velocimetry in a vertical plane along the completely rough bed surface. Experimental results indicated that flow resistance with sphere roughness is higher than that with cylindrical roughness and significant degrees of spatially regular variation in the time-averaged velocities were generated along the rough elements in case of the large ratio of the roughness height to flow depth. In addition, Reynolds shear stress and turbulent intensity abruptly decreased near the ridge of roughness elements. It was suggested that the difference in flow resistance between cylindrical roughness and sphere one, these organized flow structure were explained by form induced stress.

Keywords: open-channel shallow flow, flow resistance, rough bed, turbulent characteristics, PIV.

INTRODUCTION

Resistance coefficient for a turbulent flow over a completely rough bed in an open channel is determined by the longitudinal and cross sectional profiles of the channel; the shapes, arrangements and sizes of bed roughness elements and flow conditions. Numerous works have accumulated important knowledge. It has been revealed that in an area of a turbulent flow over a completely rough bed in a wide rectangular straight channel with the typical diameter of roughness elements being small relative to water depth and the Reynolds number sufficiently large in particular, the coefficient of friction loss can be expressed in the Prandtl-von-Karman logarithmic law. No systematic explanation has, however, yet been given concerning the coefficient of resistance for a flow with a roughness element diameter that is nearly identical to water depth. The effects of separation vortices from roughness elements on resistance characteristics of flow are also unknown (G.M.Smart *et al*, 2002). Studies have been made on the resistance characteristics of ridge and groove roughness elements as typical two-dimensional roughness elements and spot and spherical roughness elements as three-

dimensional roughness elements (Smart G.M. *et al*, 2002).

As for two-dimensional ridge roughness elements, Jean Piquet (1999) and Townsend(1976) reported that such roughness elements exhibit the characteristics of k-type roughness elements where the ratio of groove width to ridge height is 3 or higher, or of d-type roughness elements where the ratio is 1 or lower, and showed the behaviour of vortices in the groove between roughness elements and the interaction of a flow in the vortex and an external flow on a roughness element. It is also pointed out that pseudo periodic vortices are released in the groove due to pressure change caused by a large-scale vortex structure on roughness elements and that the stability of internal vortices and the pattern of internal flow vary according to the ratio of groove width to ridge height. Jimenez (2004) noted based on a flow with two-dimensional ridge roughness elements that the turbulent flow over a rough surface is governed by the roughness Reynolds number and the ratio of roughness element diameter to boundary layer thickness and that roughness affects the entire boundary layer at a ratio of not lower than 50 between roughness element diameter and boundary thickness.

Few studies have, however, compared two- and three-dimensional roughness elements as simplified artificial roughness element models in terms of resistance characteristics or internal structure of flow. Nakayama (2005) applied Direct Numerical Simulation methods (DNS) to an open channel flow with two- and three-dimensional sine waves on the bed, compared two- and three-dimensional turbulent flow over a rough surface, and reported that no variance was found in turbulent structure outside the roughness layer despite variance near the roughness element.

Ohmoto & Sukarno (2009) made measurements of flow over most closely filled spherical roughness elements with high relative roughness by using the PIV (Particle Image Velocimetry) method, a method that makes two-dimensional measurement possible. The measurements revealed that stable and highly regular upflows and downflows exist near the roughness elements. This has shown that in a flow within the roughness sublayer defined by Raupach et al., where the influence of roughness is strong, the homogeneity of the average flow and turbulence in the horizontal plane is disturbed considerably, indicating that the influence of roughness elements is very strong. It has been shown that if relative roughness is large, measured values of the resistance coefficient f derived from the Darcy–Weisbach equation tend to be slightly larger than the values of the friction coefficient derived from the logarithmic law for flow over a completely rough surface, and that the dimensionless Manning roughness coefficient is dependent on relative roughness.

It was suggested that the resistance coefficient for a turbulent flow over a completely rough surface was affected and that mass transport and momentum transport due to advection became active near the roughness elements because stable upflows and downflows occurred near roughness elements and were found to be closely correlated to main flow velocities.

In this study, aiming at comparing a turbulent flow over a completely rough surface with two- and three-dimensional roughness elements, resistance characteristics and turbulence structure near the roughness element were examined in a boundary layer for turbulence over a completely rough surface on which spherical and cylindrical roughness elements with an identical typical diameter were regularly arranged, and variances were considered.

EXPERIMENTAL APPARATUS AND METHOD

The flume used in the experiment is a circulation-type variable-slope straight flume measuring 10 m long, 40 cm wide and 20 cm high. The weir at the downstream end of the flume enables the control of water depth. The flume bed and sidewalls are made of acrylic resin so that pictures can be taken and laser beams can be emitted from the sidewalls.

A right-hand coordinate system was used. The downstream, cross-stream and upward directions are represented by x -, y - and z -axes, respectively, the corresponding mean flow velocity components by U , V and W , and the fluctuation components by u' , v' and w' . Figure 1 shows the coordinate system in detail. In this study, stainless steel cylindrical bars and glass spheres were used as cylindrical and spherical roughness elements, respectively. The bottom of an 8-m-long flume section downstream from a horizontal line 2 m from the upstream end of the flume was covered with 5-, 15- or 30-mm-diameter cylindrical bars and glass spheres. Figure 2 shows the arrangement patterns of cylindrical and spherical roughness elements.

The conditions for measuring turbulence over a rough surface using cylindrical and spherical roughness elements are listed in Table 1. Table 2 shows the experiment conditions for resistance laws for cylindrical and spherical roughness elements. The flow in the flume was kept steady by letting the water flow at a predetermined flow rate and adjusting the weir at the downstream end of the flume, and flow depth was measured with a point gauge.

The roughness Reynolds number is greater than 70 in all cases, indicating a completely rough surface. Flow velocity was measured by PIV (Particle Image Velocimetry), a representative non-contact image processing method. The measurement system is outlined in Figure 1. Measurements were taken at 4 m downstream from the upstream end of the bed surface roughened by cylindrical bars and glass spheres. An air-cooled, infrared pulse laser was used as the light source. The laser sheet beam thickness was set at 1 mm, and the pulse interval at 500 μ s. The laser beam was directed vertically downward from above the flume toward the bed of the flume. Visualization images read by synchronizing the laser beam and the CCD camera were recorded as 100 fps (frames per second), 960×1018 pixel

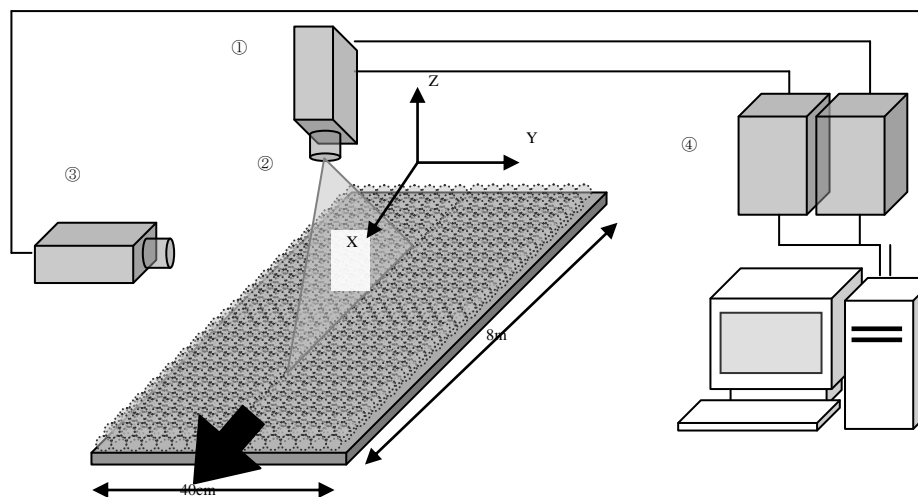
monochrome video images on the hard disk of the computer and processed by the PIV method. A lens with a focal length of 50 mm was used. The smallest pixel size was 0.06 mm. The velocity sampling frequency was 100 Hz. For each measurement plane, 2,000 images were taken, and the measurement time was 20 seconds. Nylon particles 5 μm in diameter and 1.02 in specific gravity were uniformly put into the water as tracers after putting them into an alcohol solution and stirring the solution thoroughly

RESISTANCE CHARACTERISTICS OF FLOW OVER ROUGH SURFACE

In order to compare the resistance characteristics of flow with cylindrical and spherical roughness elements, uniform flow depth was measured at the same typical diameter of the roughness element, channel gradient and quantity of flow. Some of the measurements are shown in Figure 3. Cylindrical roughness elements were most closely arranged at right angles to the main flow (Figure 2(c)) and spherical roughness elements were arranged either regularly (Figure 2(a)) or most closely (Figure 2(b)).

The depth of a uniform flow with spherical

roughness elements was greater than that with cylindrical roughness elements. The margin was evidently larger as the quantity of flow increased although there was no great variance at a quantity of flow of 1 l/sec. The value obtained by dividing the variance of uniform flow depth between the flows with cylindrical and spherical roughness elements by the depth of flow with cylindrical roughness elements was 13% for most close arrangement or 12% for regular arrangement. The depth of a uniform flow with spherical roughness elements was greater than that with cylindrical roughness elements by not less than 10%. Resistance was slightly greater in the case where spherical roughness elements were arranged most closely than where they were arranged regularly. The ratio of the projected area of spherical roughness elements in the downstream direction, a flow inhibiting area, to that of cylindrical roughness elements was 87% for closest arrangement or 79% for regular arrangement. The ratio was highest for cylindrical roughness elements followed by most closely arranged spherical roughness elements and regularly arranged spherical roughness elements.



- (1) Double-pulsed Laser Illumination system
- (2) Laser sheet
- (3) CCD-Camera kodak mega plus ES 1.0
- (4) Pulse –Laser main unit

Figure 1. Flow Measurement System

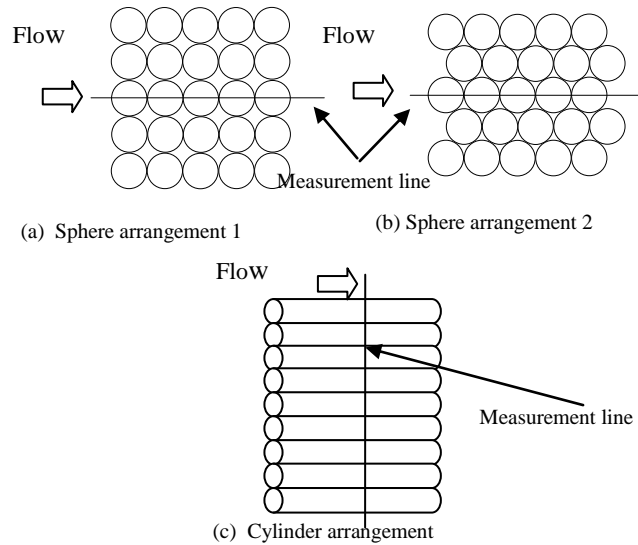


Figure 2 Bed roughness pattern and flow measurement line

Table 1 Flow measurement conditions

	Case1	Case2	Case3	Case4
Mean flow velocity U_m (cm/s)	23.9	20.5	28.4	26.2
Flow depth H(cm)	4.19	4.87	3.52	3.82
Channel slope I_0	1/500	1/500	1/500	1/500
Aspect ratio B/H	9.5	8.2	11.4	10.5
Froude Number $U_m/(gH)^{1/2}$	0.37	0.29	0.48	0.43
Reynolds Num. $U_m H/\nu$	10014	9983	9997	10000
Roughness Reynolds Num. $u_* D/\nu$	430	927	395	819
Relative roughness D/H	0.36	0.62	0.43	0.79
Roughness diameter D(mm)	15	30	15	30
Roughness shape	sphere		cylinder	

Table 2 Experimental conditions for flow resistance

D(mm)	I_0	Discharge (l/s)
15	1/500	1~10
	1/300	
30	1/500	
	1/300	

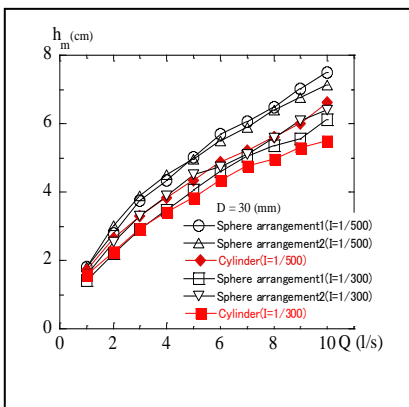


Figure 3 Relation between uniform flow depth and flow discharge

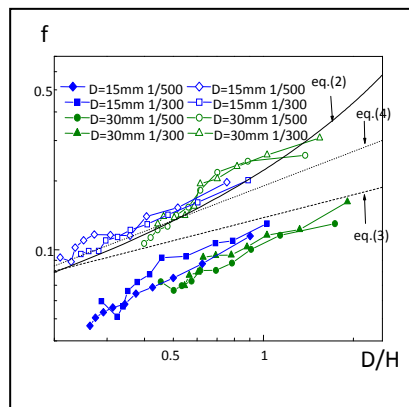


Figure 4 Resistance coefficient

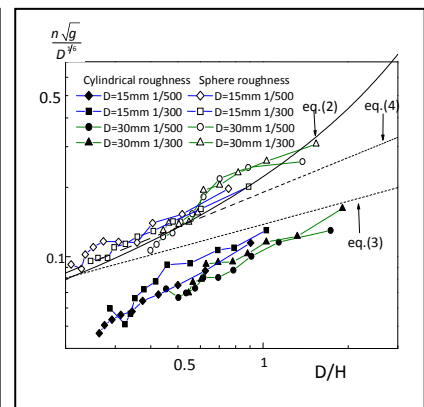


Figure 5 Manning roughness coefficient

Discussions are made below concerning the law of dimensionless resistance of flow with most closely arranged spherical roughness elements and that with cylindrical roughness elements.

The resistance coefficient f for open channel flow can be expressed, by using the Darcy–Weisbach equation, as

$$f = \frac{\tau_0}{1/8 \rho U^2} = \frac{8gh_m I_0}{U^2} \quad (1)$$

where τ_0 is the bottom shear stress; ρ , the density of water; U , cross-sectional average velocity; I_0 , channel gradient; h_m , uniform flow depth; and g , gravitational acceleration. This study focuses on resistance characteristics for spherical roughness elements with high relative roughness.

Figure 4 shows the relationship between resistance coefficient f and relative roughness. Resistance coefficient increased as relative roughness became greater either for spherical or cylindrical roughness elements.

By applying the logarithmic law to flow velocity distribution over a completely rough surface, the resistance law can be expressed as

$$\sqrt{8/f} = \frac{U}{u_*} = \frac{2.3}{\kappa} \log(h/k_s) + B_r \quad (2)$$

where k_s and B_r are the integration constants for sand-grain-equivalent roughness and a completely rough surface. These constants vary depending on the shapes, arrangements and sizes of roughness elements. For the solid line in Figure 5, $k_s = D$ and $B_r = 6.0$ were used. The resistance coefficient obtained by integrating the logarithmic law is generally in good agreement with measurements for spherical roughness elements but larger than measurements for cylindrical roughness elements. For cylindrical roughness elements, sand-grain-equivalent roughness is likely to decrease or integration constant B_r is likely to increase.

Other equations include Manning and Strickler's empirical power law

$$\sqrt{8/f} = 7.6(h/d_{50})^{1/6} \quad (3)$$

and an empirical equation of Kellerhalls derived for a gravel-bed river whose bed is very rough:

$$\sqrt{8/f} = 6.5(h/d_{50})^{1/4} \quad (4)$$

As can be seen from Figure 5, the results of calculation by the Manning–Strickler and the Kellerhalls empirical equations for spherical roughness elements show poorer agreement with measurements. Comparison of the two equations shows that the Kellerhalls equation is superior to the Manning–Strickler equation. For cylindrical roughness elements, results of both equations overestimated the measured resistance coefficient, exhibiting poor agreement.

Figure 5 shows the relationship between the dimensionless Manning roughness coefficient and relative roughness. As shown, the dimensionless Manning roughness coefficient tends to increase with relative roughness either for spherical or cylindrical roughness elements. The Manning and Strickler's empirical equation assumes that the dimensionless Manning roughness coefficient does not heavily depend on relative roughness. This assumption, however, does not hold true within the range of relative roughness covered in the experiment.

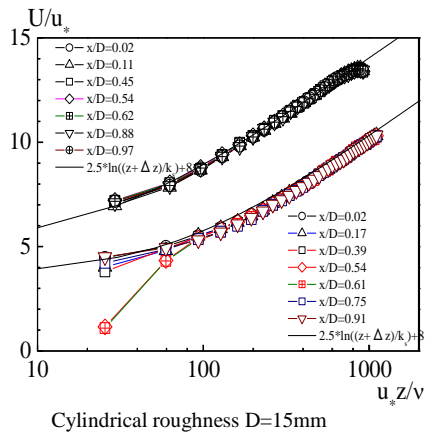
AVERAGE FLOW AND TURBULENCE CHARACTERISTICS

Figures 6 and 7 show the distribution of time-averaged flow velocity in the direction of main flow and in the vertical direction. The solid lines represent the logarithmic distribution law for a completely rough surface expressed as

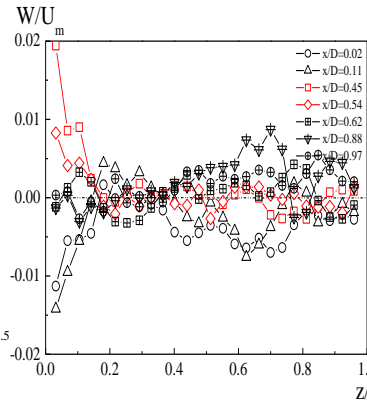
$$\frac{U}{u_*} = \frac{1}{\kappa} \ln \left(\frac{z + \Delta z}{k_s} \right) + 8.5 \quad (5)$$

where U is the time-averaged flow velocity; u_* , friction velocity; z , vertical distance from the sidewall relative to the top of the roughness element; κ , von Karman constant; k_s , sand-grain-equivalent roughness; and Δz , distance from the top of the roughness element to the virtual bed surface. Friction velocity was obtained from water depth and channel gradient under uniform flow conditions, and Δz and k_s were selected in view of agreement of the logarithmic law over a rough surface with measurements.

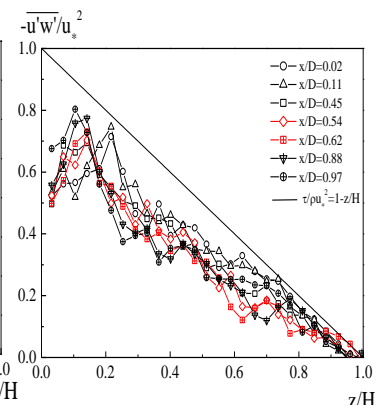
These figures show that the main flow velocity exhibits little spatial variance as the dimensionless height from the sidewall exceeds 100. Thus, the logarithmic law over a rough surface well reproduces the vertical distribution of main flow velocity except for a turbulent flow on a bed surface roughened by 30-mm-diameter spherical roughness elements



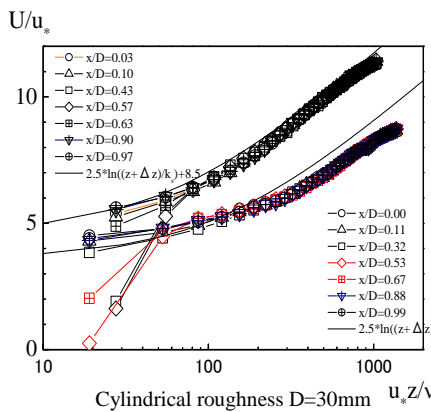
Cylindrical roughness D=15mm



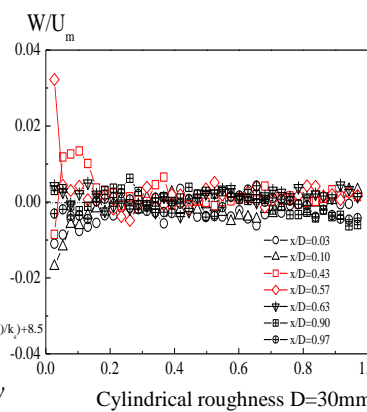
Cylindrical roughness D=15mm



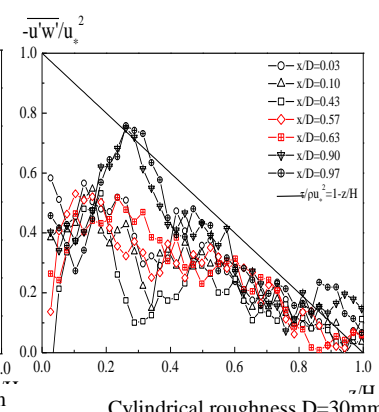
Cylindrical roughness D=15mm



Cylindrical roughness D=30mm



Cylindrical roughness D=30mm



Cylindrical roughness D=30mm

Figure 6 Vertical distribution of main flow velocity

Figure 7 Vertical distribution of secondary current W

Figure 8 Vertical distribution of Reynolds shear stress

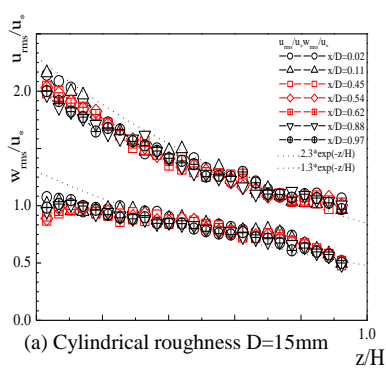
Dimensionless main flow velocity is lower in a flow with spherical roughness elements, three-dimensional elements, than in a flow with cylindrical roughness elements, two-dimensional elements; which is in agreement with the logarithmic law. The results are opposite to Nakayama's findings (2005) obtained by DNS of turbulent flows on the beds roughened by two- and three-dimensional roughness elements. The spatial variation of main flow velocity near the bed tends to be greater for spherical roughness elements than for cylindrical elements. The tendency is outstanding for 15-mm-diameter roughness elements.

The spatial variation tends to increase as roughness becomes greater for both types of roughness elements. The vertical time-averaged flow velocity component W for spherical roughness elements is large near the channel bed and decreases drastically farther away from the bed. The maximum values for upflows and downflows increase as the roughness element diameter increases. The maximum value for cylindrical roughness elements is only approximately half the value for spherical roughness elements. Bed pressure varies greatly along spherical and cylindrical roughness elements near the elements. Streamlines that are separated right downstream the top of a roughness element are attached again to another roughness element downstream. As a result, pressure

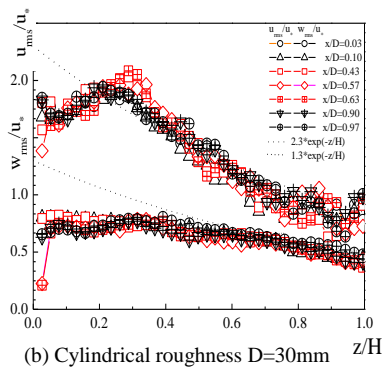
increases near the point where the streamline is attached again. The spatial change in pressure produces upflows and downflows and induces the spatial variation of main flow velocity. The vertical time-averaged flow velocity component W is correlated to the spatial variation of main flow velocity, causing vertical momentum transport. The dispersion term of momentum transport, which is closely correlated to vortex-making resistance, is described below.

Figure 8 shows vertical distributions of Reynolds shear stress for 15- and 30-mm-diameter cylindrical roughness elements. Deviation of Reynolds stress from the straight line is recognized even in a uniform flow. Deviation is outstanding near the channel bed and for 30-mm-diameter roughness elements. Red symbols are generally near the top of roughness elements and the Reynolds shear stress is considerably low near the bed.

Figure 9 shows vertical distributions of turbulence intensities in the direction of main flow and vertical direction for cylindrical roughness element diameters of 15 mm and 30 mm. The solid lines represent the turbulence intensity equation proposed by Nezu et al (1993).

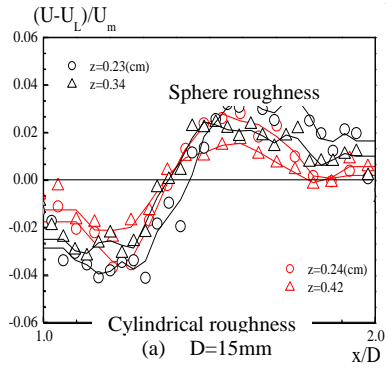


(a) Cylindrical roughness D=15mm

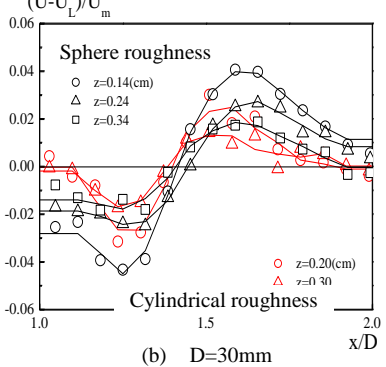


(b) Cylindrical roughness D=30mm

Figure-9 Vertical distribution of turbulent intensity

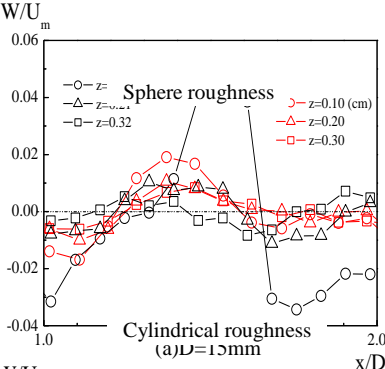


(a) D=15mm

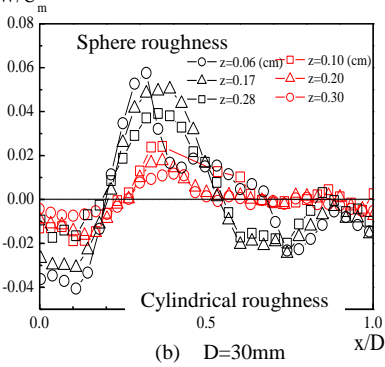


(b) D=30mm

Figure-10 Streamwise distribution of main flow velocity



(a) D=15mm



(b) D=30mm

Figure-11 Streamwise distribution of secondary current W

The turbulence intensity equation well reproduces measurements for a roughness element diameter of 15 mm except near the roughness element either for spherical Ohmoto *et al.*,(2010) or cylindrical roughness elements. Variance between calculation and measurement is great for a roughness element diameter of 30 mm. Turbulence intensity rapidly decreases near the bed because the Reynolds shear stress decreases. Upflows and downflows from near the roughness elements may be closely related to the phenomenon.

MOMENTUM TRANSPORT DUE TO ADVECTION

Shear stress $\tau(z)$ in a turbulent flow on a rough surface in the uniform flow field proposed by Nikora(2007) was given by the spatial integration of the Reynolds equation of motion between rough surface and wave length if the secondary flow of flow-depth scale can be ignored, as shown below.

$$\rho \varphi g l_0 = f_x - \frac{\partial \varphi \tau(z)}{\partial z} \tag{6}$$

$$\tau(z) / \rho = \left\langle v \frac{\partial U}{\partial z} \right\rangle - \langle u'w' \rangle - \langle U W \rangle \tag{7}$$

where f_x is material resistance in unit volume, which is zero above the top of roughness elements. Top bars and brackets represent time- and space-averaged arithmetic, respectively. Prime marks and top wavy lines represent the deviation from time average of instantaneous value, and deviation of time-averaged value from space-averaged value. The spatial deviation of main flow velocity is therefore expressed by $\tilde{u} = u - \langle u \rangle$

Vertical flow velocity component W is expressed by $\tilde{w} = w$ based on the law of mass conservation. g is gravitational acceleration; ρ , the density of water; l_0 , channel gradient; and φ , void ratio. $\varphi = 1$ above the top of roughness elements. It has been pointed out that the third term on the right side of equation (7), which is referred to as the form induced stress, is dependent upon the time-averaged flow induced by roughness elements.

Spatial variations around the roughness element of main flow velocity and of vertical flow velocity component W are shown in Figures 10 and 11. The amplitude of spatial variation of main flow velocity reached approximately 8% of that of cross sectional mean velocity for spherical roughness element diameters of 15mm and

30mm, and to approximately 4% for a diameter of 15 mm and to 7% for a diameter of 30 mm for cylindrical roughness elements. Thus, the amplitude is greater for spherical roughness elements than for cylindrical elements. The amplitude of spatial variation of vertical flow velocity component W reached approximately 7% of that of cross sectional mean flow velocity for a roughness element diameter of 15 mm and to approximately 10% of that of cross sectional mean flow velocity for a diameter of 30 mm.

The amplitude is therefore greater for spherical roughness elements than for cylindrical elements as in the case of spatial variation of main flow velocity. There generally exists negative correlation between the spatial deviation of main flow velocity and the deviation of vertical flow velocity component. The spatial deviation of main flow velocity is, however, in the positive in downflows downstream of the top of roughness elements and is close to zero where the upflows are of the maximum value. It is therefore assumed that the momentum transport into the roughness element by advection, which is similar to Reynolds shear stress, induces vortex-making resistance. Form induced stress in the third term on the right side of equation 7 is greater for spherical roughness elements than for cylindrical elements, and provides a clue for tracking down the cause of deviation of Reynolds shear stress from the linear distribution.

CONCLUSIONS

Stable upflows and downflows occur near roughness elements and are closely correlated to main flow velocities. The correlation affects the resistance law for a turbulent flow over a rough surface, mass transport and momentum transport.

In this study, aiming at comparing a turbulent flow over a completely rough surface with two- and three-dimensional roughness elements, resistance characteristics and turbulence structure near the roughness element were examined in a turbulent flow over a completely rough surface on which spherical and cylindrical roughness elements with an identical typical diameter were regularly and most closely arranged. The knowledge obtained is described below.

(1) In a turbulent flow over a completely rough surface on which spherical and cylindrical

roughness elements with the same typical diameter are regularly and most closely arranged, resistance is greater in the case with spherical roughness elements than in the case with cylindrical roughness elements.

(2) Dimensionless main flow velocity is lower in a flow with spherical roughness elements than in a flow with cylindrical roughness elements at the same dimensionless height in the area of the logarithmic law.

(3) Stable upflows and downflows occur near roughness elements in both cases with spherical and cylindrical roughness elements. The values of upflow and downflow are greater in the case of spherical roughness elements than in the case of cylindrical roughness elements.

(4) Losses from the linear distribution of Reynolds stress near roughness elements increase as the roughness element diameter become larger either for spherical or cylindrical roughness elements.

(5) In the vertical direction, the turbulence intensities u_{rms}/u^* and w_{rms}/u^* for spherical and cylindrical roughness elements are reproduced with good accuracy outside the roughness sublayer by the turbulence intensity equation using an exponential function. Near the roughness element, turbulence intensity is overestimated and the degree of agreement is reduced as the roughness element diameter increases.

(6) Form induced stress proposed by Nikora was applied to a turbulent flow over a completely rough surface on which spherical and cylindrical roughness elements were installed. As a result, it was shown that the estimated form induced stress tends to be higher for spherical roughness elements than for cylindrical roughness elements.

REFERENCES

- A. A. Townsend (1976), The structure of turbulent shear flow, 2nd ed. Cambridge Univ. Press.
- Akihiko NAKAKAYA(2005), Study of Instantaneous and Filtered Flow Field Near the Bed of Open- Channel Flow by DNS, Annual Journal of Hydraulic

- Engineering, JSCE, Vol.50, pp.757-762, .
- Iehisa Nezu, Hiroji Nakagawa (1993), Turbulence in open-channel flows, IAHR. , Balkema, pp.57-58.
- Jean Piquet (1999), Turbulent Flow –Models and Physics, Springer, pp.652-672.
- Javier Jimenez (2004), Turbulent Flows Over Roughwalls, Annual. Rev. Fluid Mech., Vol.36, pp.173-196.
- Ohmoto T. & Sukarno T. (2010), Shallow turbulent flow over regularly arrayed sphere roughness in an open channel, Proceedings of the 6th International Symposium on Environmental Hydraulics, Athens, Greece, Environmental Hydraulics Vol.1, pp.99-104.
- Smart G.M., Duncan M.J. and J.M.Walsh (2002), Relative Rough Flow Resistance Equations, J. Hydraulic Engineering, Vol.128, No.6, pp.568-578.
- Vladimir Nikora et al. (2007) , Double-Averaging Concept for Rough-Bed Open-Channel and Overland Flows, Journal of Hydraulic Engineering, Vol. 133, No. 8, ASCE 2007.